Transition to a new tetragonal phase of WO_3: crystal structure and distortion parameters

1999 J. Phys.: Condens. Matter 11 4143

(http://iopscience.iop.org/0953-8984/11/21/303)

J. Phys.: Condens. Matter **11** (1999) 4143–4156. Printed in the UK PII: S0953-8984(99)01549-0

Transition to a new tetragonal phase of WO_3: crystal structure and distortion parameters

K R Locherer†, I P Swainson‡ and E K H Salje†

† Department of Earth Sciences and IRC in Superconductivity, University of Cambridge, Cambridge CB2 3EQ, UK
‡ NPMR, SIMS, NRC, Chalk River Laboratories, Chalk River, ON, Canada KOJ 1J0

E-mail: krl21@esc.cam.ac.uk, Ian.Swainson@nrc.ca and es10002@esc.cam.ac.uk

Received 2 February 1999

Abstract. At 1100 K a new phase of WO_3 with space group $P4/ncc$, $a = 5.2885(5)$ Å and $c = 7.8626(8)$ Å, was established, and its crystal structure was determined. The previously known tetragonal phase $P4/nmm$, which is shown to exist only above 1170 K, was also refined with $a = 5.3031(4)$ Å and $c = 3.9348(3)$ Å at 1200 K. The difference between the two perovskite-like structures relates to a tricritical non-ferroic transition characterized by a soft mode at the Z-point of the Brillouin zone, which induces antiphase rotations of the WO_6 octahedra about [001]. The oxygen sublattice of the lower tetragonal structure is shown to possess the symmetry of the $a^0a^0c^-$ perovskite tilt structure $F4/mmc$ ($I4/mcm$), which is violated by the off-centre antiferroelectric displacements of the tungsten atoms that lead to the observed space group $P4/ncc$.

1. Introduction

In recent decades a large amount of research has been directed towards tungsten trioxide single crystals and thin films, after it was suspected to be ferroelectric [1]. More recently WO_3 has attracted attention due to its polarons and bipolarons, which made it a well behaved substitute for studies of the similar electronic structure of the high temperature superconductor $YBa_2Cu_3O_{7-\delta}$ [2, 3]. Thin films of WO_3 were also envisaged for electrochromic device applications when doped with protons [4–6]. Tetragonal Na_xWO_3 ($0.28 \leqslant x \leqslant 0.35$) has been known to be superconducting for a long time [7, 8], while superconductivity has also been reported for a cubic variant ($0.16 \leqslant x \leqslant 0.4$) [9]. More recently slightly oxygen reduced WO_3 was found to exhibit sheet superconductivity [10]. The crystal structure of that phase was determined by Aird *et al* [11].

The structure of tetragonal WO_3 at 1223 K was first solved by Kehl *et al* [12] using powder x-ray diffraction. The space group was given as $P4/nmm$, with the tungsten position at $(\frac{1}{4}, \frac{1}{4}, z_W = 0.06)$ and the oxygen position at $(\frac{1}{4}, \frac{1}{4}, z_O = z_W + \frac{1}{2})$. It was noticed by several authors [12–16] that there are anomalies in the thermal expansion and strong expansion of the a-axis of the tetragonal phase between 1140 K and 1170 K. The suspicion appears in a number of publications (e.g. Sawada [16]) that a phase transition takes place. However no structural change was found previously.

It is the purpose of this paper to show that an additional tetragonal phase of WO_3 exists at 1100 K, to present its crystal structure and to discuss the structural differences with the previously know tetragonal structures.

0953-8984/99/214143+14$19.50

2. Experiment

Material for the powder diffraction experiments were obtained in two steps. A platinum crucible was filled with 99%+ pure WO_3 powder of 20 μm grain size (Aldrich, cat no 23278-5) and placed in a furnace at 1073 K for 100 h [17]. The temperature was then raised to 1723 K for about two hours. The furnace was then turned off and left to cool to room temperature. From the surface of the recrystallized mass, crystals with plate-like habit (parallel to 001) were recovered. These were then ground in acetone.

The neutron scattering experiments were performed at the C2 diffractometer at Chalk River Laboratories. Two spectra were taken, at 1100 K and 1200 K. The wavelength used was $\lambda = 1.3288$ Å. A broad background peak near $2\theta = 23^\circ$ and some smaller ones at higher angles were removed because they could be identified as scattering of the beam by parts of the furnace. The spectra in figures 1 and 2 show the only difference to be the appearance of extra peaks at temperatures between 1200 K and 1100 K. These signals, near $2\theta = 35^\circ$, 56°, 71° and 85° are superlattice reflections. They can be understood as being caused by a doubling of the *c* lattice parameter, as already suggested by Roth and Waring [18]. Kehl *et al* [12] determined the space group of the tetragonal phase as $P4/nmm$. Accordingly an attempt was made to refine both phases within that space group. This was unsuccessful, which indicated that at least one of the space groups was incorrectly assigned. Only for the higher temperature spectrum did the refinement reproduce the observed intensities. Alternative space groups were then derived for the lower temperature spectrum from extinction rules and group theoretical considerations.

The problem for the assignment of a space group symmetry lies in the fact that only two peaks disappear visibly when the crystal undergoes the transition between the two tetragonal phases. For the weaker reflections it is not straightforward to determine whether their intensities exceed the background noise. Table 1 shows the peaks identified as being present. The strongest

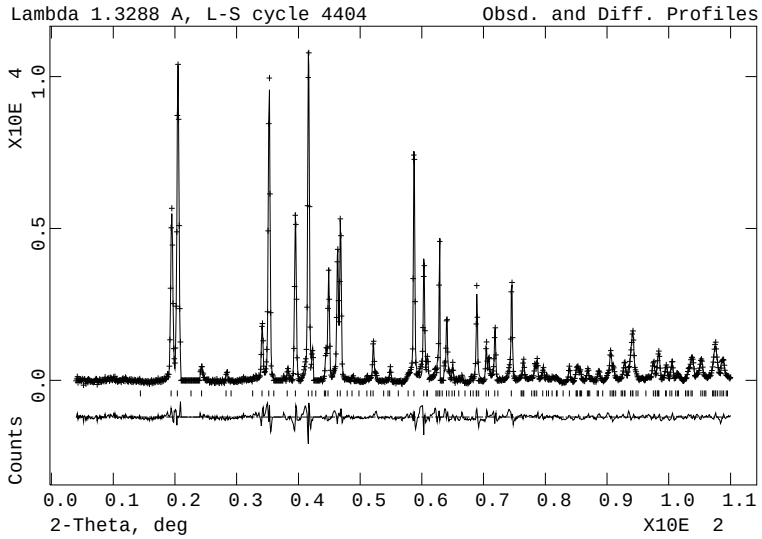

Figure 1. Observed, calculated and difference powder neutron diffraction profiles for WO_3 at 1100 K. This pattern belongs to the $P4/ncc$ phase.

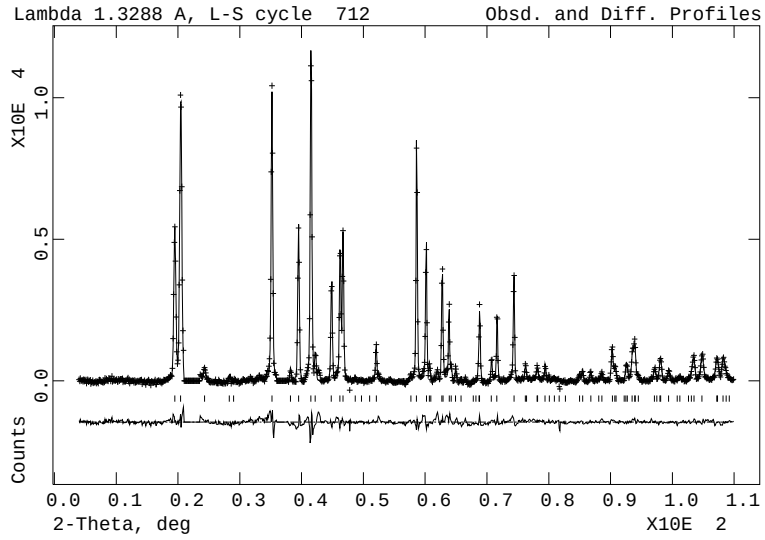

Figure 2. Observed, calculated and difference powder neutron diffraction profiles for WO_3 at 1200 K. This pattern belongs to the $P4/ncc$ phase.

Table 1. Extinctions for the lower tetragonal phase. Question marks denote reflections/conditions that are uncertain.

Class of reflection	Observed reflections	Conditions
hkl	321, 215, 314, 324	no condition
$hk0$	310, 510	$h + k = 2n$
$h0l$	102, 202, 104, 302, 106, 402, 206, 404	$l = 2n$
$h00$	400	?
hhl	110, 112, 221 ?, 222, 224, 330, 116, 334	$l = 2n$?
$00l$	002, 004, 008	$l = 2n$

support was for the extinction rule $00l; l = 2n$, $h0l; l = 2n$ which corresponds to three space groups, $P4_2cm$, $P\bar{4}c2$ and $P4_2/mcm$. If the weaker condition $hhl; l = 2n$ is included, the space groups $P4cc$ and $P4/mcc$ are possible. With $hk0; h + k = 2n$ and $h00; h = 2n$ the space group becomes $P4_2/ncm$. If all the conditions are included the space group is $P4/ncc$.

Two criteria were applied to identify the relevant space group. Firstly, since the very minor difference between the diffraction patterns suggests that the structural changes are subtle, no major deviations from the puckered structure of the $P4/nmm$ phase are to be expected. This condition was imposed by selecting space groups that are subgroups of $P4/nmm$. Secondly, the model must refine to good statistical factors R_{wp}, R_p and χ^2.

No group relationship exists between $P4/nmm$ and $P4_2/mcm$, and $P4/nmm$ and $P4/mcc$. These were therefore discarded. $P4_2/ncm$ is a subgroup of index two, while $P4_2cm$ and $P4cc$ are subgroups of index four. Although these space groups reproduce the structure they do not give satisfactory refinements. $P\bar{4}c2$ is a subgroup $P4/nmm$ of index four. There are three possible intermediate groups, $P\bar{4}m2$, $P4_2/ncm$ and $P4/ncc$. All three pathways lead to two possible configurations of $P\bar{4}c2$. Either the Wyckoff positions [8j] and

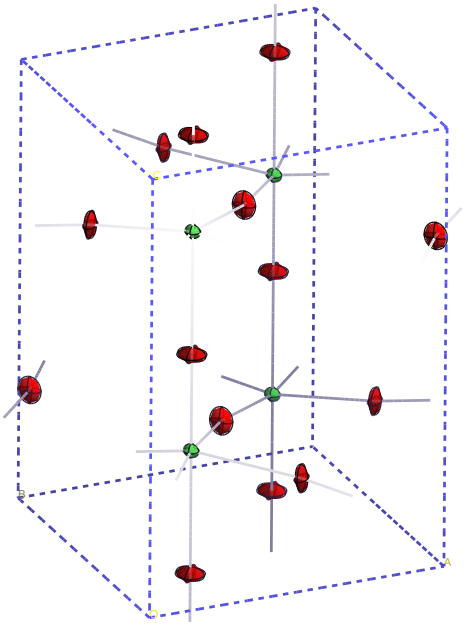

Figure 3. Thermal ellipsoid plot of the tetragonal $P4/ncc$ structure.

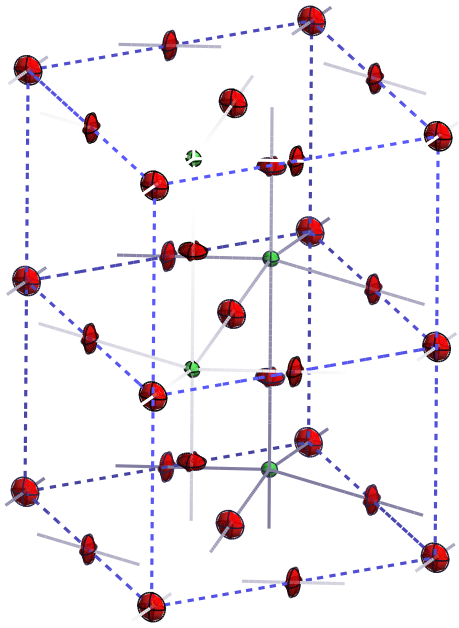

Figure 4. Thermal ellipsoid plot of the tetragonal $P4/nmm$ structure. Two unit cells stacked along [001] are shown.

[4i] are occupied, or the positions [4f], [4e] and [4i]. The latter gives a satisfactory refinement. However, on closer examination it was revealed that the two oxygen positions on [4e] and [4f] coincide within error. If these positions are restrained to be the same the symmetry is $P4/ncc$. This does not adversely affect the refinement, and thus $P4/ncc$ was adopted as the 'correct' space group.

The appropriate transformation matrix between $P4/nmm$ and $P4/ncc$ is [19]

$$T_Z = \left[\begin{array}{ccc|c} 1 & 0 & 0 & 0 \\ 0 & 1 & 0 & 0 \\ 0 & 0 & 2 & \frac{1}{2} \end{array}\right] \tag{1}$$

giving the correct c-axis doubling. Thus the transformation proceeds via a Z-point transition (figure 5).

The refinements of the two space groups were performed using the code GSAS [20]. The absorption was calculated for a cylindrical sample holder of 0.5 cm diameter, assuming a packing fraction of $\frac{1}{2}$, as 0.11 cm^{-1}. For both phases, five profile parameters (the Gaussian peak width coefficients U, V and W, the Lorentzian peak width coefficient Y and the asymmetry coefficient A_s), sixteen Chebychef background coefficients, the zero-point, the scale factor and two lattice parameters were used. Additionally, three fractional coordinates and eight anisotropic temperature factors were refined in the $P4/ncc$ phase. 142 Bragg reflections were generated, giving an overdetermination ratio of over 13.

For the $P4/nmm$ phase two fractional coordinates and eight anisotropic temperature factors were refined. 80 Bragg reflections were generated, giving an overdetermination ratio of just over eight.

The R-factors achieved were $R_{wp} = 4.76$, $R_p = 3.42$ and $\chi^2 = 4.637$ for $P4/ncc$ and $R_{wp} = 4.75$, $R_p = 3.35$ and $\chi^2 = 4.540$ for $P4/nmm$. The refined parameters are given in

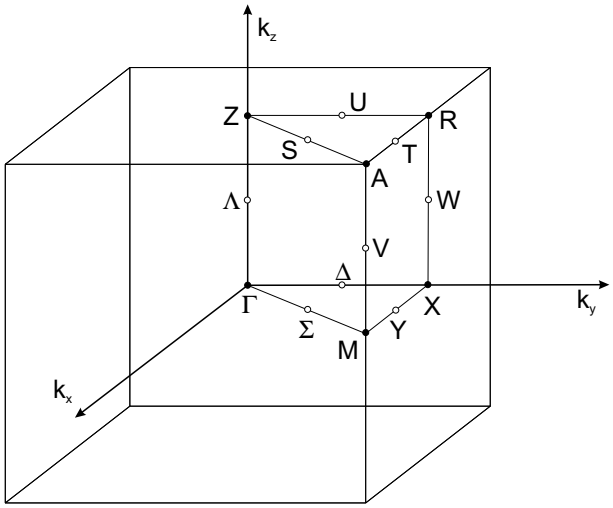

Figure 5. The Brillouin zone for tetragonal P: $\Gamma = (0, 0, 0)$, $M = (\frac{1}{2}, \frac{1}{2}, 0)$, $Z = (0, 0, \frac{1}{2})$, $A = (\frac{1}{2}, \frac{1}{2}, \frac{1}{2})$, $R = (0, \frac{1}{2}, \frac{1}{2})$, $X = (0, \frac{1}{2}, 0)$. The transition from $P4/nmm$ to $P4/ncc$ is associated with the Z point.

Table 2. The refined parameters for $P4/ncc$. The thermal parameters have been multiplied by 100.

Atom	x	y	z	U_{iso}	u_{11}	u_{22}	u_{33}	u_{12}	u_{13}	u_{23}
W^1	0.2500	0.2500	0.2832(4)	1.53	1.6(1)	1.6(1)	1.4(2)	0.0	0.0	0.0
O^1	0.2500	0.2500	0.0030(5)	4.36	5.7(2)	5.7(2)	1.6(2)	0.0	0.0	0.0
O^2	−0.0249(1)	0.0249(1)	0.2500	3.58	2.49(9)	2.49(9)	5.6(2)	−1.4(1)	−0.2(1)	−0.2(1)

Table 3. The refined parameters for $P4/nmm$. The thermal parameters have been multiplied by 100.

Atom	x	y	z	U_{iso}	u_{11}	u_{22}	u_{33}	u_{12}	u_{13}	u_{23}
W^1	0.2500	0.2500	−0.0664(8)	1.49	1.5(1)	1.5(1)	1.5(2)	0.0	0.0	0.0
O^1	0.2500	0.2500	0.4940(9)	4.45	5.7(2)	5.7(2)	2.1(2)	0.0	0.0	0.0
O^2	0.0000	0.0000	0.0000	4.32	3.40(9)	3.40(9)	6.2(2)	−2.2(1)	0.1(1)	0.1(1)

tables 2 and 3. Plots of the refined structure are shown in figures 3 and 4. Bond information is listed in tables 4 and 5.

3. Temperature dependence of I and e

A series of long wavelength ($\lambda = 2.3717$ Å) neutron diffraction patterns were taken between room temperature and 1210 K. Using the Pawley method [21] in FULLPROF [22] both the lattice parameters (table 6) and the observed intensity of the disappearing superlattice peak (211) were extracted from this series.

The extracted intensity was normalized by the intensity of the (202) peak, which does not change in the transition. The resulting intensity versus temperature is plotted in figure 6. A

Table 4. Bond lengths and bond angles for $P4/ncc$.

Vector	Length	Angle	Degrees
W^1-O^1	2.203(5)	O^1-W^1-O^1	180.0
W^1-O^1	1.728(5)	O^1-W^1-O^2	82.1(1) × 4
W^1-O^2	1.897(2) × 4	O^1-W^1-O^2	97.9(1) × 4
		O^2-W^1-O^2	88.9(3) × 4
		O^2-W^1-O^2	164.2(2) × 2

Table 5. Bond lengths and bond angles for $P4/nmm$.

Vector	Length	Angle	Degrees
W^1-O^1	1.730(5)	O^1-W^1-O^1	180.0
W^1-O^1	2.205(5)	O^1-W^1-O^2	97.9(1) × 4
W^1-O^2	1.8930(5) × 4	O^1-W^1-O^2	82.1(1) × 4
		O^2-W^1-O^2	88.91(3) × 4
		O^2-W^1-O^2	164.1(2) × 2

Table 6. The lattice parameters refined for the tetragonal phases using the Pawley method in FULLPROF. The data for the two phases are seperated by the horizontal line at 1181 K.

T (K)	a (Å)	c (Å)
1030(3)	5.2730(6)	7.8422(8)
1040(3)	5.2742(3)	7.8467(4)
1050(3)	5.2749(2)	7.8480(3)
1060(3)	5.2749(1)	7.8480(2)
1070(3)	5.2765(3)	7.8505(4)
1080(3)	5.2775(2)	7.8512(3)
1090(3)	5.2786(2)	7.8522(3)
1100(3)	5.2795(3)	7.8530(4)
1110(3)	5.2804(2)	7.8539(3)
1120(3)	5.2814(3)	7.8543(4)
1131(3)	5.2827(3)	7.8552(5)
1141(3)	5.2842(3)	7.8555(4)
1151(3)	5.2871(3)	7.8558(4)
1161(3)	5.2911(3)	7.8552(4)
1170(3)	5.2937(3)	7.8564(5)
1181(3)	5.2948(2)	3.9284(1)
1190(3)	5.2955(3)	3.9293(2)
1200(3)	5.2954(3)	3.9298(2)
1210(3)	5.2956(2)	3.9306(1)

linear fit of the type

$$I^2 = I_0^2(T_c - T) \tag{2}$$

between the temperatures 1090 K and 1160 K leads to the values of $T_c = 1170(94)$ K and $I_0^2 = 9.9(6) \times 10^{-4}$ K^{-1}.

Since the intensity scales with the square of the order parameter [23] this suggests that the transition is tricritical. Note that a continuous transition is compatible with the super-subgroup relation between the two phases.

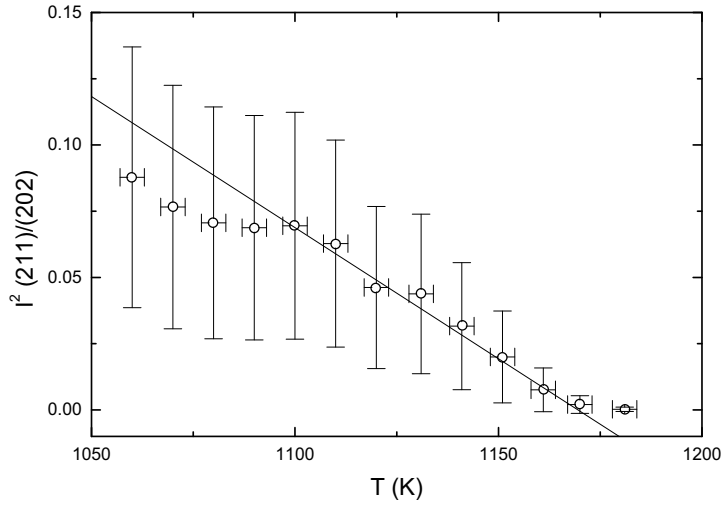

Figure 6. The square of the intensity of the superlattice reflection (211) versus temperature in WO_3. The straight line represents a least squares fit between 1090 K and 1160 K.

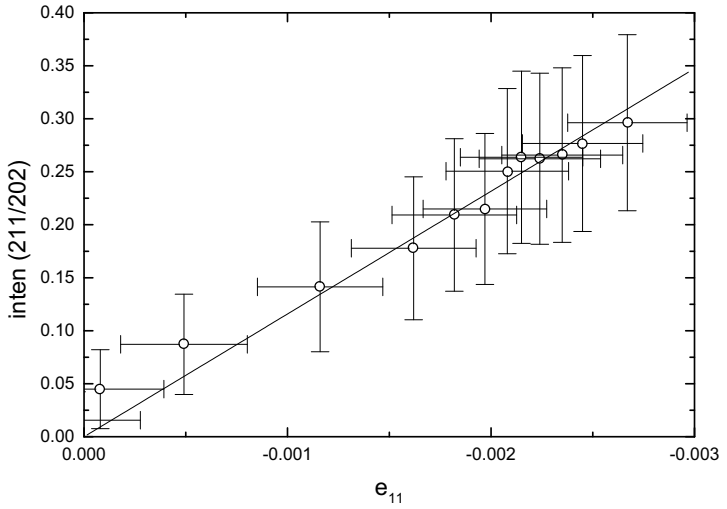

Figure 7. The intensity of the superlattice reflection (211) versus the strain e_{11} for the transition $P4/nmm$ to $P4/ncc$ in WO_3. The straight line represents a least squares fit, constrained by the origin.

In addition, the strain (figure 8) was extracted by extrapolating the a-axis lattice parameter from the $P4/nmm$ phase into the $P4/ncc$ phase and then applying the formula

$$e_{11} = a/a_0 - 1 = e_{22}. \tag{3}$$

Since there is no change in the crystal class the strain is not symmetry breaking. In figure 7 it can be seen that the strain is proportional to the intensity of the (211) reflection. As both scale with respect to the same symmetry constraints, this observation implies that the strain is proportional to the square of the order parameter. This is consistent with a zone boundary transition.

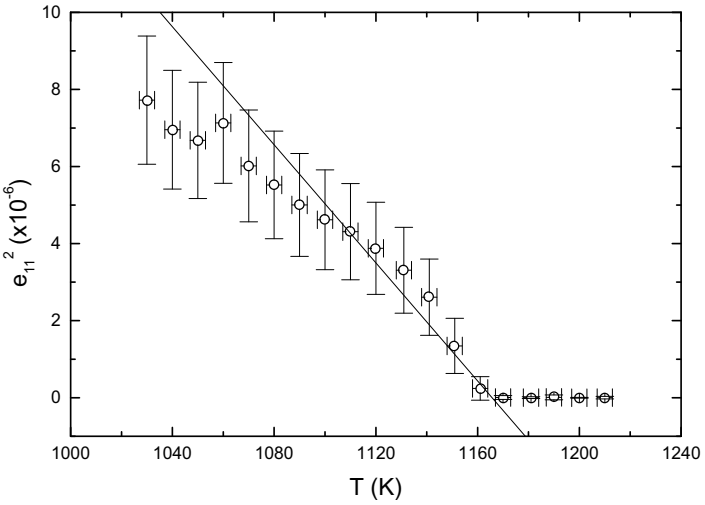

Figure 8. The square of the tetragonal–tetragonal strain e_{11} versus temperature in WO_3. The straight line represents a least squares fit between 1090 K and 1160 K.

Figure 8 shows that the e_{11} strain can be fitted using

$$e_{11}{}^2 = e_{11,0}{}^2(T_c - T) \tag{4}$$

with $T_c = 1165(95)$ K and $e_{11,0}{}^2 = 7.7(6) \times 10^{-8}\ \mathrm{K}^{-1}$. Thus the transition temperature agrees with the values found for the intensity above.

Also, there is a very small strain in the c-axis, given by

$$e_{33} = c/c_0 - 1. \tag{5}$$

This is plotted in figure 9. The magnitude of this strain is so small no attempt was made to fit the data and extract the transition temperature.

It should be noted that although it is possible to describe the transition as tricritical within error it is probably slightly first order. This is supported by the specific heat results obtained by Sawada [16], which show a small cusp at the transition.

4. The transition

To shed more light on the underlying mechanism of this phase transition the atomic coordinates for the series of long wavelength spectra were refined between 1050 K and 1200 K using the GSAS code. Overall 20 parameters were fitted for the $P4/ncc$ phase: the zeropoint of 2θ, four Chebychef polynomial background coefficients, two lattice parameters, four profile parameters (the Gaussian peak width U, V, W and the Lorentzian peak width Y), six atomic parameters (with isotropic thermal motion) and a scale factor. For the $P4/nmm$ phase 17 parameters were refined. There are 31 and 17 reflections respectively, and the refinements converged at typically $R_{wp} = 0.09$, $R_p = 0.07$ and $\chi^2 = 2.0$. In both refinements the overdetermination ratio is over three.

The result is given in figures 10 and 11. The equivalent of an atomic order parameter was evaluated according to

$$Q_{atomic} = \sqrt{(x - x_0)^2 + (y - y_0)^2} \tag{6}$$

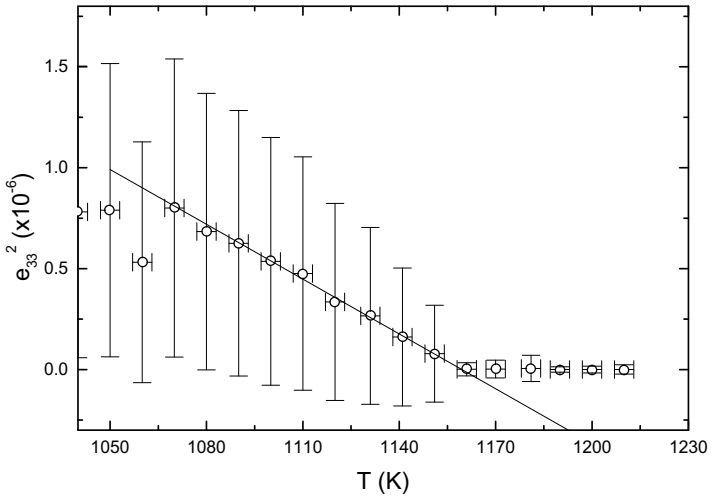

Figure 9. The square of the tetragonal–tetragonal strain e_{33} versus temperature in WO_3. Ignore the point at 1040 K, which is too near the tetragonal–orthorhombic transition. The straight line represents a least squares fit.

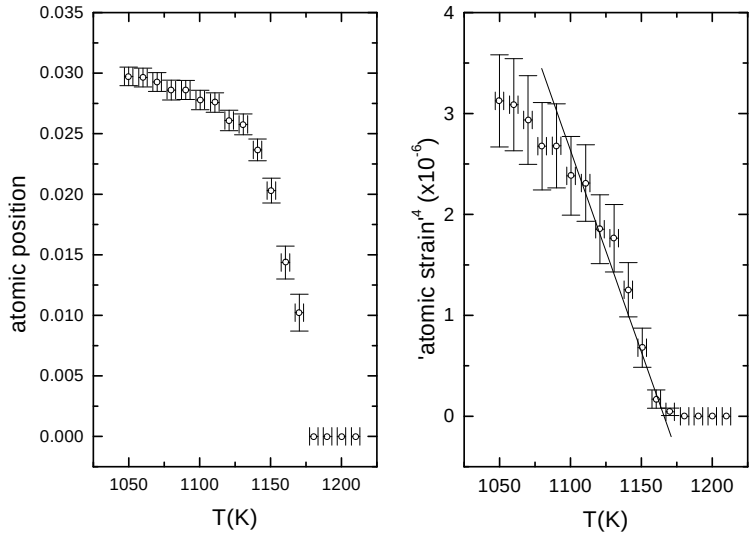

Figure 10. Left: the variation of the atomic positions for the second oxygen position. Right: the fourth power of the atomic strain calculated directly from the atomic positions for O^2 versus temperature. The straight line represents a least squares fit of the atomic strain between 1090 K and 1160 K.

where $x = -y$ is the atomic position of the basal oxygen (O^2) in the low symmetry phase. The x_0 and y_0 are the atomic positions in the high symmetry phase, the special position $(0, 0, 0)$. The atomic order parameter thus measures the displacement of the atoms from their high symmetry position.

A fit of the order parameter according to

$$Q_{atomic}{}^4 = Q_{atomic,0}{}^4(T_c - T) \tag{7}$$

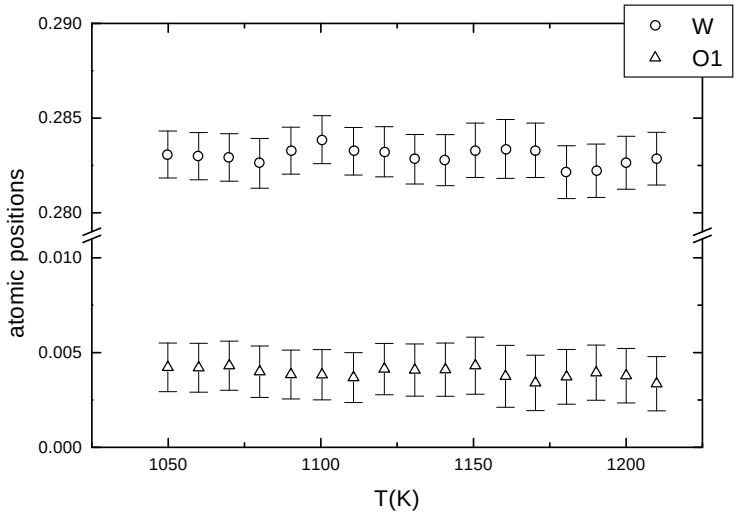

Figure 11. The variation of the z component of the atomic coordinates for the W and O^1 atom versus temperature in WO_3 The fractional coordinates refer to the $P4/ncc$ unit cell.

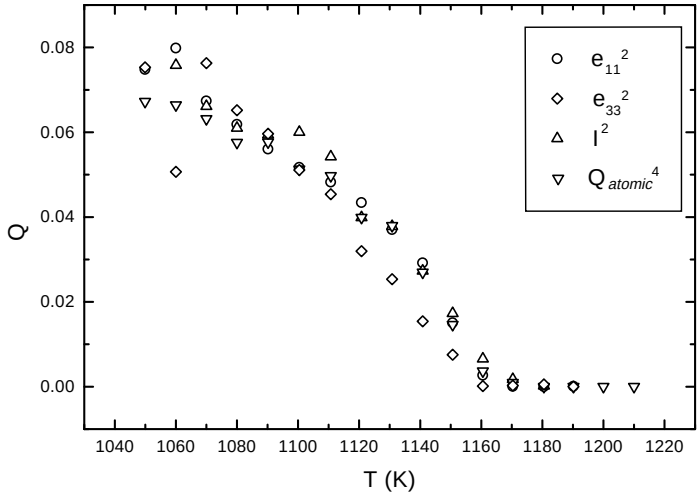

Figure 12. The order parameter for the $P4/nmm$ to $P4/ncc$ transition.

produced $T_c = 1171(61)$ K and $Q_{atomic,0}{}^4 = 4.0(3) \times 10^{-8}$ K^{-1}. This is in agreement with what was found for the macroscopic strain above. The order parameter is plotted in figure 12. Below 1090 K the order parameter saturates. This may be explained by the approach to the tetragonal–orthorhombic phase transition.

The full symbols for the two tetragonal space groups are $P4/n\,2_1/m\,2/m$ and $P4/n\,2_1/c\,2/c$. Hence the transition involves the loss of the mirror planes in (100) and (110). These symmetry elements are violated by the displacements of the basal oxygens from the special position (0, 0, 0) in $P4/nmm$ to $(0-\delta_1, 0+\delta_1, \frac{1}{4})$ in $P4/ncc$. This results from a soft mode at the Z-point of the Brillouin zone (figure 5), which induces antiphase rotations of the oxygen polyhedra about [001] (figure 13). The rotations cause the expansion e_{11} in the basal plane.

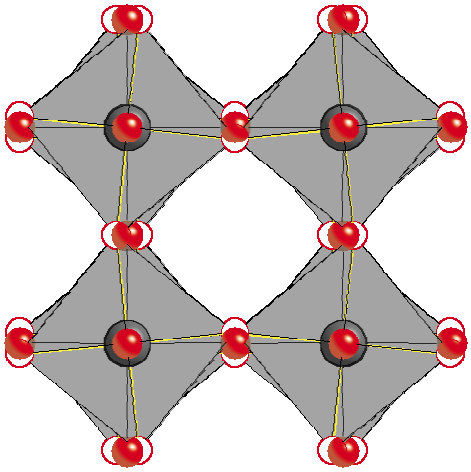

Figure 13. Displacements of the basal oxygens between the two tetragonal phases. The positions of the atoms in $P4/nmm$ are indicated as solid spheres, while the hollow spheres represent the distorted structure of $P4/ncc$. The transition produces pure shears in opposite directions for the $z = 1/4$ and $z = 3/4$ layers. Hence the macroscopic strain does not break the symmetry of the unit cell in the basal plane.

A measure of the distortion of the octahedra is given by the mean octahedral elongation and the octahedral angle variance [24]

$$\langle\lambda_{oct}\rangle = \frac{1}{6}\sum_{i=0}^{6}(l_i/l_0)^2 \tag{8}$$

$$\sigma_{oct}^2 = \frac{1}{11}\sum_{i=0}^{12}(\theta_i - 90^\circ)^2 \tag{9}$$

where l_i are the centre-to-apex distances and θ_i are the octahedral angles of the strained octahedron, while l_0 is centre-to-apex distance in a perfect octahedron. This was worked out for both structures using the program VOLCAL [25]. It was found that $\langle\lambda_{oct}\rangle = 1.019$ and $\sigma_{oct} = 6.82^\circ$ for $P4/nmm$, while $\langle\lambda_{oct}\rangle = 1.019$ and $\sigma_{oct} = 6.78^\circ$ for $P4/ncc$. The numbers give an idea of how strongly the octahedra are distorted from the $m3m$ symmetry of the parent phase $Pm\bar{3}m$.

The lack of distortion between the two tetragonal phases reconfirms that only octahedral rotations are involved in the transition. The two phases can be classified within the Glazer scheme of tilted octahedra in perovskites [26]. As such $P4/nmm$ belongs to the zero-tilt system $a^0a^0a^0$ of unit cell $a_p \times b_p \times c_p$, with $a_p = b_p = c_p$. This corresponds to the parent phase $Pm\bar{3}m$. The reduction of symmetry is due solely to the distortions of the octahedra caused by the displacement of the tungsten atoms.

On the other hand $P4/ncc$ belongs to the one-tilt system $a^0a^0c^-$ of unit cell $2a_p \times 2b_p \times 2c_p$, with $a_p = b_p < c_p$. The corresponding space group is $F4/mmc$ (or $I4/mcm$), if the distortion were to take place in a perovskite. Again, the symmetry reduction is a result of the displaced tungsten atoms. The two phases $P4/nmm$ and $P4/ncc$ are thus related by the octahedral rotation c^- through γ, which is synonymous with the 'atomic order parameter' Q defined above,

$$Q = \tan\gamma \approx \gamma = \frac{x}{0.25} = Q_0' x. \tag{10}$$

According to [26] the dimensions of the unit cell are then given by

$$a_p = \xi \cos\gamma, \qquad b_p = \xi \cos\gamma, \qquad c_p = \xi \tag{11}$$

where ξ is the anion-anion distance through the centre of the octahedron.

Comparisons can be drawn to the soft modes at the R-point of the cubic phase of the perovskites $SrTiO_3$ at 110 K [27, 28] and $KMnF_3$ ([29], and references therein) at 184 K, which result in the predicted symmetry of the $a^0a^0c^-$ tilt system. It appears that in WO_3 a similar transition sequence would be observed, if it were not for the soft mode at the M-point of the (hypothetical) $Pm\bar{3}m$ parent phase that breaks the symmetry before an R-point transition to $F4/mmc$ can take place. A number of other materials with the same tilt structure are given in table 7, showing that the angle γ observed in WO_3 is average.

Table 7. Materials displaying the $a^0a^0c^-$ perovskite tilt structure. References: (*a*) [31]; (*b*) this study; (*c*) [29]; (*d*) [32]; (*e*) [33]; (*f*) [34]; (*g*) [35]. Temperatures for $MAgF_3$ are not known to the authors.

Material	SG	γ	T_{obs} (K)	T_c (K)
$SrTiO_3$[(a)]	$F4/mmc$	1.4°	77	110
WO_3[(b)]	$P4/ncc$	5.6°	1100	1171
$KMnF_3$[(c)]	$F4/mmc$	9.1°	145	184
$BaBi_{1-x}Pb_xO_3$ ($x = 0.8$)[(d)]	$F4/mmc$	7.3°	295	$\approx$ 600
$Pr_{1-x}Ba_xMnO_3$ ($x = 0.35$)[(e)]	$F4/mmc$	8.7°	210	300
$SrZrO_3$[(f)]	$F4/mmc$	6.4°	1173	1443
$MAgF_3$ (M = Rb, Cs)[(g)]	$F4/mmc$	4.6°	n/a	n/a

5. Comparison to the tetragonal room temperature phase in WO_3

More recently experiments on slightly oxygen reduced WO_{3-x} ($x \approx 0.1$) have been performed by Aird *et al* [11] and Aird and Salje [10]. Single crystals of WO_3 were reduced by placing them with sodium metal at opposite ends of a sealed evacuated U-shaped silica tube. This assemblage was then heated to 730 K for varying amounts of time [11]. The Na vapour was transported to the WO_3 and reduced the surface while forming Na_2O. The high oxygen mobility within the sample then resulted in a subsequent reduction of the sample further from the surface, according to Aird *et al* [11]. Sheet superconductivity was then observed in some of the samples [10]. One of the reduced crystals was used to perform single crystal x-ray diffraction to refine the bulk structure.

It was found that the symmetry of the system is $P\bar{4}2_1m$, and the unit cell has the size $a = 7.39$ Å and $c = 3.88$ Å. It is thus twice as large as the $P4/nmm$ cell, but has the same volume as the $P4/ncc$ cell. Similarities can be seen in table 8. Both $P\bar{4}2_1m$ and $P4/ncc$ are subgroups of $P4/nmm$, but there is no such relation between them. $P4/nmm$ corresponds with $P\bar{4}2_1m$ via an M-point transition. The transformation matrix is [19]

$$T_M = \left[\begin{array}{ccc|c} 1 & \bar{1} & 0 & \frac{\bar{1}}{4} \\ 1 & 1 & 0 & \frac{1}{4} \\ 0 & 0 & 1 & 0 \end{array}\right]. \tag{12}$$

Here the point group changes from $4/mmm$ to $\bar{4}2m$, and the centre of symmetry is lost. Thus this phase is expected to be piezo-electric. The octrahedral elongation $\langle\lambda_{oct}\rangle = 1.060$, the angle variance is $\sigma_{oct} = 13.49°$, the mean bond length is 1.9105 Å and the bond length variance

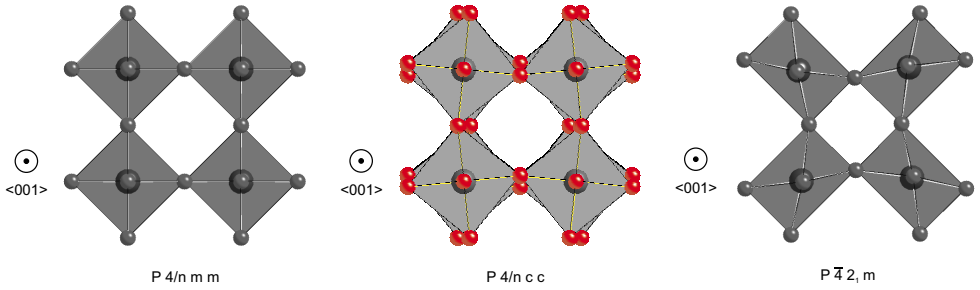

Figure 14. From left to right: the $P4/nmm$, $P4/ncc$ and $P\bar{4}2_1m$ structure viewed along ⟨001⟩. Note the antiphase rotations of the WO_6 octahedra about the c-axis for the $P4/ncc$ phase and the strong octahedral distortions of the $P\bar{4}2_1m$ phase. The W atoms are represented by the larger spheres and are partly covered by the smaller O atoms.

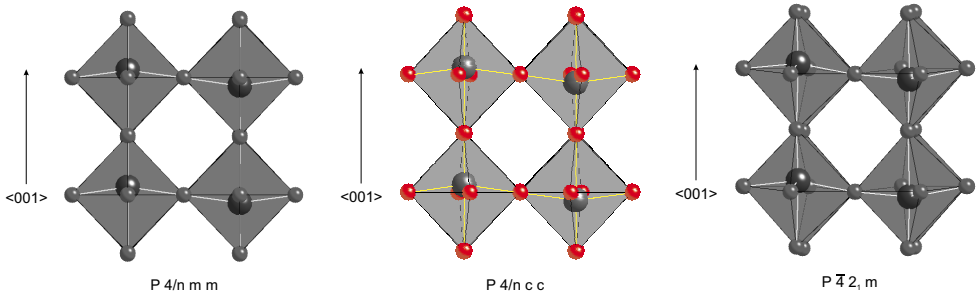

Figure 15. From left to right: the $P4/nmm$, $P4/ncc$ and $P\bar{4}2_1m$ structure. ⟨001⟩ is in the plane of the paper, pointing up. The tungsten displacements are practically the same for all phases.

is $\sigma_{bond} = 0.026$ Å. The strong distortion of the octahedra is apparent from figures 14 and 15, in which the three tetragonal variants of WO_3 are compared. The displacement patterns of the tungsten atoms are broadly the same for all three structures. The main differences lie in the distortions of the oxygens. While there is only a slight difference between $P4/nmm$ and $P4/ncc$, the oxygens in $P\bar{4}2_1m$ are distorted so strongly in the (001) plane that octahedra have a distinctive rectangular shape. This is re-emphasized when viewing the structure along the plane containing ⟨001⟩.

Table 8. Table of the atomic parameters for the three tetragonal phases of WO_3. Data for $P\bar{4}2_1m$ taken from Aird *et al* [11].

Atom	x	y	z	U_{iso}	Space group
W^1	0.2529(1)	0.7569(1)	−0.0698(2)	0.0183(2)	$P\bar{4}2_1m$
	0.2500	0.7500	−0.0666(8)	0.0176	$P4/nmm$
	0.2500	0.7500	−0.0664(8)	0.0197	$P4/ncc$
O^1	0.263(4)	0.763(4)	0.493(5)	0.070(7)	$P\bar{4}2_1m$
	0.2500	0.7500	0.4948(8)	0.0468	$P4/nmm$
	0.2500	0.7500	0.4970(9)	0.0496	$P4/ncc$
O^2	0.002(2)	0.792(2)	0.024(5)	0.042(6)	$P\bar{4}2_1m$
	0.000	0.7500	0.0000	0.0462	$P4/nmm$
	−0.0249(3)	0.7500	0.000	0.0541	$P4/ncc$

Acknowledgments

The authors thank Ron Donaberger and Michael Watson for help with the experimental equipment at Chalk River. KRL would like to thank Magdalene College, Cambridge, and the EPSRC for financial support. Further assistance was provided by the European Community, the National Research Council of Canada and the Department of Earth Sciences, Cambridge.

References

[1] Matthias B 1949 *Phys. Rev.* **76** 430
[2] Salje E 1994 *Eur. J. Solid State Inorg. Chem.* **31** 805
[3] Salje E K H, Rehmann S, Pobell F, Morris D, Knight K S, Herrmannsdörfer T and Dove M T 1997 *J. Phys.: Condens. Matter* **9** 6563
[4] Granqvist C 1992 *Solid State Ionics* **53–56** 479
[5] Granqvist C 1994 *Solar Energy Materials and Solar Cells* **32** 369
[6] Pham Thi M and Velasco G 1985 *Revue de Chimie Minérale* **22** 195
[7] Raub C, Sweedler A, Jensen M, Broadston S and Matthias B 1960 *Phys. Rev. Lett.* **13** 746
[8] Shanks H 1974 *Solid State Commun.* **15** 753
[9] Garifyanov N, Khlebnikov S, Khlebnikov I and Garifullin I 1996 *Czech. J. Phys.* **46** 855
[10] Aird A and Salje E 1998 *J. Phys.: Condens. Matter* **10** 377
[11] Aird A, Domeneghetti M, Mazzi F, Tazzoli V and Salje E 1998 *J. Phys.: Condens. Matter* **10** 569
[12] Kehl W, Hay R and Wahl D 1952 *J. Appl. Phys.* **23** 212
[13] Brækken H 1969 *Det Kongelige Norske Videnskabers Selskabs Forhandlinger* **42** 25
[14] Ackermann R and Sorrell C 1970 *High Temp. Sci.* **2** 119
[15] Sawada S 1956 *J. Phys. Soc. Japan* **11** 1237
[16] Sawada S 1956 *J. Phys. Soc. Japan* **11** 1246
[17] Salje E 1977 *Acta Crystallogr.* B **33** 574
[18] Roth R and Waring J 1966 *Journal of Research, National Bureau of Standards* A **70** 281
[19] Stokes H and Hatch D 1988 *Isotropy Subgroups of the 230 Crystallographic Space Groups* 1st edn (Singapore: World Scientific)
[20] Larons A and v Dreele R 1994 *GSAS - General Structure Analysis System* LANSCE, MS-H805, Los Alamos National Laboratory, NM 87545, USA
[21] Pawley G 1981 *J. Appl. Crystallogr.* **14** 357
[22] Rodriquez-Carvajal J 1993 *FULLPROF* Institut Laue-Langevin, Laboratoire Leon Brillouin (CEA-CNRS)
[23] Cowley R 1981 Landau Theory *Structural Phase Transitions. Monograph on Physics* eds A D Bruce and R A Cowley (London: Taylor and Francis)
[24] Robinson K, Gibbs G and Ribbe P 1971 *Nature* **172** 567
[25] Finger L 1979 *VOLCAL — Program to Calculate Polyhedral Volumes and Distortion Parameters* Carnegie Institution of Washington, Washington DC, USA
[26] Glazer A 1972 *Acta Crystallogr.* B **28** 3384
[27] Cowley R, Buyers W and Dolling G 1969 *Solid State Commun.* **7** 181
[28] Shirane G and Yamada Y 1969 *Phys. Rev.* **177** 858
[29] Minkiewicz V, Fujii Y and Yamada Y 1970 *J. Phys. Soc. Japan* **28** 443
[30] Nye J 1985 *Physical Properties of Crystals* 2nd edn (Oxford: Oxford University Press)
[31] Unoki H and Sakudo T 1967 *J. Phys. Soc. Japan* **23** 546
[32] Marx D, Radaelli P, Jorgensen J, Hitterman R, Hinks D, Pei S and Dabrowski B 1992 *Phys. Rev.* B **46** 1144
[33] Jirak Z, Pollert E, Andersen A, Grenier J and Hagenmuller P 1990 *Eur. J. Solid State Inorg. Chem.* **27** 421
[34] Ahtee M, Glazer A and Hewat A 1978 *Acta Crystallogr.* B **34** 752
[35] Odenthal R and Hoppe R 1971 *Monatshefte der Chemie* **102** 1340